X-ray photon pairs with highly suppressed background

D. Borodin,[1] A. Schori,[1] F. Zontone,[2] and S. Shwartz[1]
[1]*Physics Department and Institute of Nanotechnology, Bar Ilan University, Ramat Gan, 52900 Israel*
[2]*ESRF – The European Synchrotron, 71, Avenue des Martyrs 38000, Grenoble, France*
(Received 9 March 2016; published 25 July 2016)

We describe an experiment demonstrating the possibility to generate collinear indistinguishable x-ray photon pairs with a highly suppressed background. By choosing angles near 90 degrees between the detectors and the pump beam, where the pump polarization is in the scattering plane, we improve the signal-to-noise ratio by 2 orders of magnitude. We measure the pure coincidence spectrum without any energy discrimination with a bandwidth of 1.5 keV at the full width at half maximum.

DOI: 10.1103/PhysRevA.94.013843

Parametric down conversion (PDC) is a second-order nonlinear process in which a pump photon decays into two photons, which are commonly called signal and idler. One of the most important applications of PDC in the optical regime is as a source for the generation of nonclassical states of light, such as entangled photons and squeezed light [1]. The extension of quantum optics into the x-ray regime would open new possibilities for research that would most-likely gain from the existence of commercial detectors with nearly 100% detection efficiency and with photon-number-resolving capabilities.

The effect of x-ray PDC was first discussed by Freund and Levine in 1969 [2]. However, although Eisenberger and McCall observed parametric decay of x-ray photons into two lower-energy x-ray photons in 1971 [3], only a few experiments in this regime have been reported [4–6]. Several experiments in a different regime—x-ray into x-ray and ultraviolet (UV) photons—have been reported revealing important properties of the nonlinear susceptibility at UV energies and visualizing of local optical response [7–9]. In recent years several quantum effects in the x-ray regime have been demonstrated, for example, modulation of single γ photons [10], collective Lamb shift [11], and electromagnetically induced transparency [12]. A method for generating Bell states at x-ray wavelengths by using PDC was proposed in 2011 [13]. However, despite the advantages of PDC over other methods, no evidence for such nonclassical states of x-ray radiation using PDC has been reported yet. There are several major challenges that hamper the use of x-ray PDC as a source for research in the field of quantum optics: (1) the pump photons are Compton scattered into almost any direction. Since the cross section of Compton scattering in a typical experiment is about 10^5 higher than the cross section of PDC, a non-negligible portion of the Compton scattered photons is registered erroneously as PDC photons by the detection electronics. Moreover, Compton scattering limits the input flux to a level at which the Compton scattering rate is much smaller than the inverse of the dead time of the detectors. Thus Compton scattering restricts the enhancement of the rate of x-ray pairs generated via PDC. (2) A large number of quantum optics effects, such as the Hong-Ou-Mandel effect [14] and the Bell inequality [15], could be advanced if the emerging generated signal and idler photons were collinear and indistinguishable. However, momentum conservation (phase matching) for collinear x-ray PDC is very near the Bragg condition, and since the strength of Bragg scattering is orders of magnitude stronger than the strength of PDC, collinear x-ray photons have never been observed. (3) The bandwidth of x-ray PDC is predicted to be on the order of several keV [6], while x-ray optical components (except from detectors) have bandwidths narrower than a few hundred eV.

In this paper we describe and demonstrate experimentally how to suppress Compton and Bragg scattering while increasing the coincidence count rate of the photon pairs that are generated by PDC. We measured maximum coincidence count rate of about 0.1 pairs/s, which is almost an order of magnitude higher than any previous experiments. The signal-to-noise ratio (SNR) in the present experiment is about 2 orders of magnitude higher than previous reports [5,6]. We measured x-ray pair count rates when the deviation from the Bragg angle is only 0.0086° (about the FWHM of the rocking curve) and where the angle between the centers of the two detectors is only 2.3° with no significant Bragg scattering.

Similar to the visible regime, in x-ray PDC the pump and the generated photons must satisfy energy conservation, which can be written as $\hbar\omega_p = \hbar\omega_s + \hbar\omega_i$. The indices p,s, and i represent the pump, the signal, and the idler, respectively. Since x-ray wavelengths are comparable to the distances between the atomic planes, phase matching can be achieved by using the reciprocal lattice vector $\vec{G}$ [2]. The phase-matching diagram is shown in Fig. 1(a) and the phase-matching equation is expressed as $\vec{k}_p + \vec{G} = \vec{k}_s + \vec{k}_i$, where k denotes the wave vector of the corresponding photon.

Because of the weak dispersion in the x-ray regime, the magnitudes of phase-matching angles for the frequency-degenerate idler and signal are very close to the Bragg angle. Consequently, the phase-matching angles for the collinear degenerate signal and idler are within the rocking curve of the Bragg diffraction. Since in most cases Bragg scattering is much stronger than PDC, the observation of the collinear signal and idler photons requires the suppression of Bragg scattering.

To understand our approach to eliminating Bragg and Compton scattering, we recall that for photon energies that are far below the rest mass of the electron and high above the binding energies of the electrons in the generating crystal the microscopic differential cross sections for Compton scattering and Bragg scattering are approximately the Thomson cross section. This cross section approaches zero when the angle between the detector and the input beam is 90° and the input beam polarization is in the scattering plane [16]. As a result,

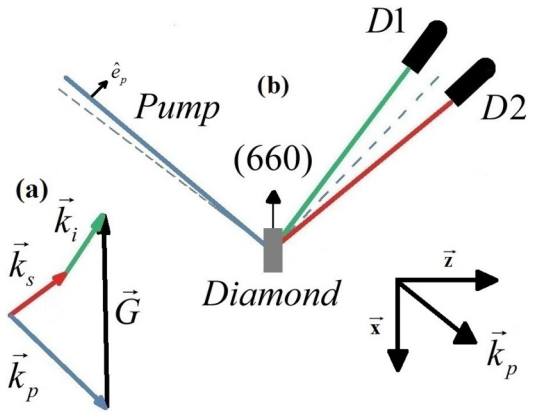

FIG. 1. (a) Phase-matching scheme. (b) Schematic of the experimental setup. The indices p,s, and i are for the pump, signal, and idler, respectively, $\vec{G}$ represents the reciprocal lattice vector orthogonal to the (660) atomic planes, and $\hat{e}$ is a polarization vector. $D1$ and $D2$ indicate the two detectors.

under these conditions both Compton and Bragg scattering are highly suppressed.

The nonlinearity that dominates at x-ray wavelengths is a plasmalike nonlinearity [3,17]. A nonuniform charge density distribution and the Lorentz force are the essence of the second-order nonlinearity, even in centrosymmetric crystals. The nonlinear current density is given by [13]

$$J_s^{NL} = -\frac{q\rho_G\omega_s E_p E_i^*}{2m^2\omega_p^2\omega_s^2\omega_i^2}[\omega_i\omega_p(\vec{G}\cdot\hat{e}_s)(\hat{e}_p\cdot\hat{e}_i) - \omega_i\omega_s(\vec{G}\cdot\hat{e}_p)(\hat{e}_i\cdot\hat{e}_s) + \omega_p\omega_s(\vec{G}\cdot\hat{e}_i)(\hat{e}_p\cdot\hat{e}_s)], \quad (1)$$

where q and m are the electron charge and mass. E_j, ω_j, and $\hat{e}_j$ are the electric field envelope, the frequency, and the polarization vector of the corresponding photon. $\rho_0(\vec{r}) = \rho_G \exp(i\vec{G}\cdot\vec{r})$ is the unperturbed charge density, where ρ_G is Fourier component of the charge density corresponding to the reciprocal lattice vector $\vec{G}$. From Eq. (1) it is seen that at a scattering angle near 90° the second term is much larger than the other terms on the right-hand side of the equation. In this case the current density is approximated to

$$J_s^{NL} = \frac{q\rho_G E_p E_i^*}{2m^2\omega_p^2\omega_i}(\vec{G}\cdot\hat{e}_p)(\hat{e}_i\cdot\hat{e}_s). \quad (2)$$

It is very clear from Eq. (2) that unlike the cross sections for Compton and Bragg scattering, the nonlinear current density is non-negligible, when pump polarization in the scattering plane and angles between the source and the detector close to 90°. Hence under these conditions, we expect to measure x-ray pairs with negligible background. We note that a similar approach has been used recently in a work demonstrating the effect of nonlinear Compton scattering [18]. We also note that similar to Bragg scattering, the nonlinear scattering is proportional to the Fourier component of the electron density corresponding to the chosen reciprocal lattice vector. However, unlike Bragg scattering it is also proportional to the magnitude of the reciprocal lattice vector. Thus, although the Fourier component decreases at higher-order reflections, the dependence on the reciprocal lattice vector moderates the reduction of the nonlinear current at higher-order reflections. Consequently, we can choose the pump photon energy to be high enough to reduce the undesired effects of loss.

The slowly varying envelope coupled equations for the frequency domain signal and idler operators in the Heisenberg-Langevin picture can be written as [6]

$$\frac{\partial a_s}{\partial z} + \frac{\alpha_s}{\cos\theta_s}a_s = \kappa' a_i^+ \exp(i\Delta k_z z) + \sqrt{\frac{2\alpha_s}{\cos\theta_s}}f_s,$$
$$\frac{\partial a_i^+}{\partial z} + \frac{\alpha_i}{\cos\theta_i}a_i^+ = \kappa'^* a_s \exp(-i\Delta k_z z) + \sqrt{\frac{2\alpha_i}{\cos\theta_i}}f_i^+, \quad (3)$$

where a_s,a_i are the signal and the idler annihilation operators; θ_s, θ_i are the signal and the idler angles, with respect to the atomic planes, obtained from the solution of the phase matching; α_s, α_i are the absorption coefficients at the signal and idler frequency, respectively; and $\kappa' = \frac{i\kappa}{\sqrt{\cos\theta_s\cos\theta_i}}$, where κ is the nonlinear coupling coefficient. The nonlinear coupling coefficient is connected to the envelope of the nonlinear current density via the relations $\kappa = -(2\hbar\eta_p\eta_s\eta_i\omega_p\omega_s\omega_i)^{\frac{1}{2}}\varepsilon_0\frac{iJ_s^{NL}}{2\varepsilon_0\omega_s E_i^*}$, where η_j is the wave impedance at the corresponding frequency. $\Delta k_z = k_p\cos\theta_p - k_s\cos\theta_s - k_i\cos\theta_i$ is the phase mismatch. The terms f_s, f_i are the Langevin noise operators. Another theoretical approach that leads to similar results was derived by Dorfman and Mukamel [19]. The coincidence count rate is defined as

$$R_c = A\iint\langle a_i^+(\vec{r}_2,t_2)a_s^+(\vec{r}_1,t_1)a_s(\vec{r}_1,t_1)a_i(\vec{r}_2,t_2)\rangle d\vec{u}d\tau, \quad (4)$$

where A is the effective spot size of the pump, $\vec{u} = \vec{r}_2 - \vec{r}_1$ and $\tau = t_2 - t_1$, and the indices 1 and 2 refer to the detector $D1$ and detector $D2$, respectively.

The experiment described here was conducted at beamline ID-10 of the European Synchrotron Radiation Facility. The schematic of the experimental setup is shown in Fig. 1(b). A monochromatic pump beam at a photon energy of 21 keV illuminates a high-quality diamond crystal with dimensions of 4 mm × 4 mm × 0.8 mm in transmission (Laue) geometry. We use the reciprocal lattice vector normal to the C(660) atomic planes for phase matching. The angle that satisfies the Bragg condition for those atomic planes is 44.73°. The generated signal and idler photons are collected by two silicon drift detectors with a diameter of 5.6 mm located 800 mm from the crystal. The average input intensity is 2×10^{12}photons/s. We estimate that the polarization ratio between the in-plane and the out-of-plane polarizations of the pump beam is about 10^3. The coincidence electronics records only photons that hit the two detectors within a time window of 370 ns. Next, we scan through the data and apply the following rule as a photon energy filter for each of the coincidence events: the sum of the energies from the two detectors equals the pump energy within an energy window of 500 eV. All experimental data are corrected for air absorption.

First we measure the detector count rates when the crystal and the detectors are at the phase-matching angles. The average total count rate is about $(2.21\pm0.05)\times10^3$photons/s at detector $D1$ and $(2.12\pm0.05)\times10^3$photons/s at detector $D2$. The typical spectrum is shown in Fig. 2. The narrow peak

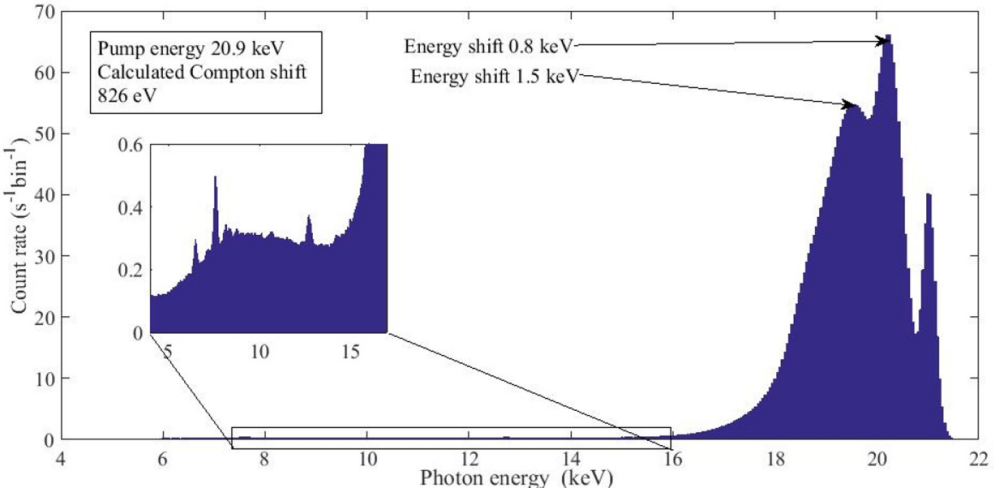

FIG. 2. Typical raw spectrum measured by a single detector. The Compton peak is at the calculated photon energy. The possible nature of the second Compton-like peak is discussed in the text. The inset shows the structure at the energies of interest. Several fluorescence peaks originated mainly from elements such as iron and lead are clearly seen in the range of 6-15 keV.

on the right is the elastic scattering; the second peak with an energy shift of 800 eV is the Compton scattering (the calculated Compton shift is 826 eV). The broad peak with the energy shift of 1.5 keV is not well understood and its explanation is rather speculative. One of the possibilities is that the photon loses its kinetic energy on the K edge of the silicon in the detector. Another possible mechanism is multiple scattering: the photon is being backscattered by the Compton mechanism with a shift of about 1.6 keV and then Bragg reflected in the direction of the detector. We estimate the energy resolution at 21 keV to be about 400 eV according to the FWHM of the elastic peak.

Next, we measure the coincidence count rate. By using a setup where the angles between the source and the detectors are near 90°, we reduced the Compton count rate to its minimal values. This allows us to choose the deviation angle of the pump from the Bragg angle to be as small as the FWHM of the rocking curve and thus increase the PDC count rate. It is important to note that the deviation angle in the present experiment is limited only by the physical dimensions of the detectors, which restricts the possibilities for phase matching.

Energy histograms at the frequency-degenerate phase-matching case for the angular separation of 2.3° between the detectors are shown in Fig. 3. The degenerate case is defined as $\omega_s = \omega_i = \omega_{s0}$, where $\hbar\omega_{s0}$ is the degenerate photon energy. Here, panels (a) and (b) correspond to the first and the second detector, respectively. Of importance, even without applying the energy filter described above it is seen that the peaks corresponding to the PDC effect are pronounced. The total count rate obtained 0.149 ± 0.003 pairs/s. The photon energy filter removes the accidental coincidence Compton counts. The PDC count rate after applying the filter is 0.088 ± 0.002 photons/s with a bandwidth of than 1.5 keV at the FWHM. The theory described above predicts a bandwidth of about 3.5 keV at the FWHM and a count rate of 2.6 pair/s.

Figure 4 shows energy histograms at the off-degenerate phase matching after applying the photon energy filter. Here, panels (a) and (b) correspond to the off-degenerate conditions of $\omega_s/\omega_{s0} = 1.2$ and $\omega_s/\omega_{s0} = 1.4$, respectively. As we move further away from the degeneracy the coincidence

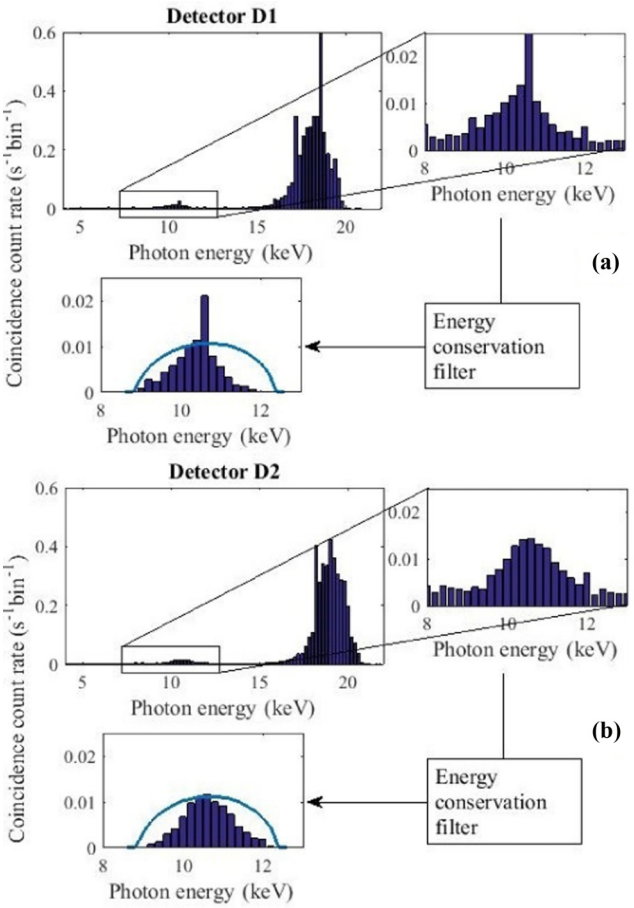

FIG. 3. Energy histograms of the measured coincidence count rate at the degeneracy for detectors $D1$ and $D2$ are depicted on (a) and (b), respectively. Raw coincidence data and results of applying the energy conservation filter, i.e., the sum of the energies of each coincidence event equals the pump energy within an energy window of 500 eV. Solid lines are theoretical calculations.

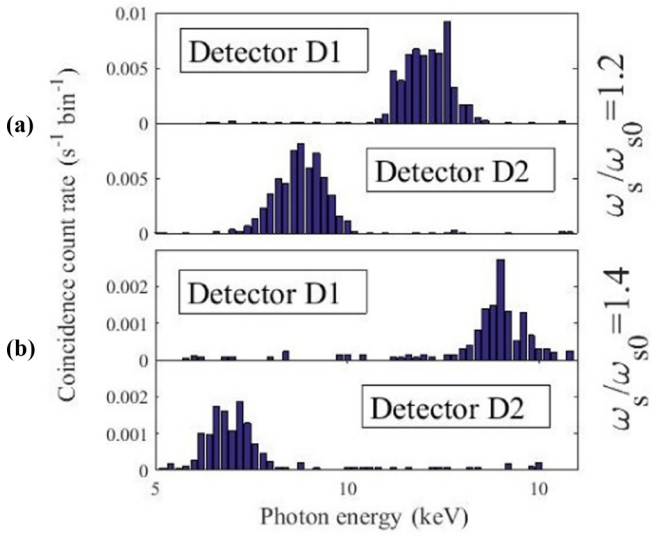

FIG. 4. Coincidence diagrams after applying the energy conservation for the off-degeneracy cases (a) $\omega_s/\omega_{s0} = 1.2$ and (b) $\omega_s/\omega_{s0} = 1.4$.

count rate drops down. At $\omega_s/\omega_{s0} = 1.2$ we measure 0.058 ± 0.002 pairs/s and at $\omega_s/\omega_{s0} = 1.4$ only 0.012 ± 0.001 pairs/s. In the latter case, the PDC signal is outweighed by the Compton tail and it is observed only with the photon energy filter. The divergence in coincidence count rate between the theory and the experiment is about a factor of 20. The model assumes that the pump is a plane wave whereas in reality it has a finite width. In addition, the theory does not take into account the overlap between the pump and the generated beams and the rich temporal structure of the beams. We define the SNR as the ratio between the PDC and the Compton count rate at the selected by phase matching spectral region. The obtained SNR is 113 for the degenerate energy.

In conclusion, we have demonstrated how to generate x-ray photon pairs with negligible background by using a geometry where the angles between the pump and the emerging photons are nearly 90° and the pump polarization is in the scattering plane. The maximum coincidence count rate was about 0.1 pairs/s and the Compton count rate was about 2×10^3 photons/s, whereas in the previous work described in Ref. [6] the highest count rate of PDC was 0.025 pairs/s and the Compton count rate is about 2×10^4 photons/s for an input intensity of 2×10^{11} photons/s. Such a significant background suppression allowed us to measure the actual coincidence count rates without any energy discrimination. Consequently, in contrast to all previous reports, in the present work the coincidence count rates at the degeneracy do not depend on the choice of the energy discrimination and the energy histograms we have described in this paper represent the true spectra of the coincidence counts. Our results can be further improved with a higher ratio between the polarizations of the input beam. This can be achieved either by using undulators with better polarization ratio or by using x-ray polarizers before the generating crystal. Since by using the geometry we present here Compton scattering is greatly reduced, the input intensity can be increased substantially without saturating the detectors. Finally, since in the geometry we describe here Bragg scattering is highly suppressed as well, our experiment shows a way to generate collinear indistinguishable x-ray pairs via PDC. This can lead to the observation of quantum optics effects such as the Hong-Ou-Mandel effect with x rays. It is interesting to note that the theoretical calculation of the coincidence count rate of the collinear signal and idler predicts that the temporal width of the biphoton wave function can be shorter than 100 attoseconds. This is shorter than any previously discussed biphoton wave functions and it is enabled by the very large pump frequency and the very weak dispersion in the x-ray regime.

This work was supported by the Israel Science Foundation (ISF) (under Grant No. 1038/13). D.B. gratefully acknowledges support by the Ministry of Aliyah and Immigrant Absorption of Israel. We acknowledge the European Synchrotron Radiation Facility for provision of synchrotron radiation facilities. The authors thank Bernhard Adams and David Reis for useful discussions.

[1] D. Bouwmeester, A. Ekert, and A. Zeilinger, *The Physics of Quantum Information: Quantum Cryptography, Quantum Teleportation, and Quantum Computation* (Springer, New York, 2000).
[2] I. Freund and B. F. Levine, Phys. Rev. Lett. **23**, 854 (1969).
[3] P. M. Eisenberger and S. L. McCall, Phys. Rev. Lett. **26**, 684 (1971).
[4] Y. Yoda, T. Suzuki, X.-W. Zhang, K. Hirano, and S. Kikuta, J. Synchrotron Radiat. **5**, 980 (1998).
[5] B. Adams, *Nonlinear Optics, Quantum Optics, and Ultrafast Phenomena with X-Rays* (Kluwer Academic Publisher, Boston, MA, 2008).
[6] S. Shwartz, R. N. Coffee, J. M. Feldkamp, Y. Feng, J. B. Hastings, G. Y. Yin, and S. E. Harris, Phys. Rev. Lett. **109**, 013602 (2012).
[7] K. Tamasaku, K. Sawada, and T. Ishikawa, Phys. Rev. Lett. **103**, 254801 (2009).
[8] K. Tamasaku, K. Sawada, E. Nishibori, and T. Ishikawa, Nat. Phys. **7**, 705 (2011).
[9] B. Barbiellini, Y. Joly, and K. Tamasaku, Phys. Rev. B **92**, 155119 (2015).
[10] F. Vagizov, V. Antonov, Y. V. Radeonychev, R. N. Shakhmuratov, and O. Kocharovskaya, Nature (London) **508**, 80 (2014).
[11] R. Röhlsberger, K. Schlage, B. Sahoo, S. Couet, and R. Rüffer, Science **328**, 1248 (2010).
[12] R. Röhlsberger, H.-C. Wille, K. Schlage, and B. Sahoo, Nature (London) **482**, 199 (2012).
[13] S. Shwartz and S. E. Harris, Phys. Rev. Lett. **106**, 080501 (2011).
[14] C. K. Hong, Z. Y. Ou, and L. Mandel, Phys. Rev. Lett. **59**, 2044 (1987).
[15] J. S. Bell, Physics **1**, 195 (1964).
[16] D. Atwood, *Soft X-Rays and Extreme Ultraviolet Radiation: Principles and Applications* (Cambridge University Press, Cambridge, UK, 1999).
[17] Y. R. Shen, *The Principles of Nonlinear Optics* (John Wiley & Sons, New York, 2003).
[18] M. Fuchs *et al.*, Nat. Phys. **11**, 964 (2015).
[19] K. E. Dorfman and S. Mukamel, Phys. Rev. A **86**, 023805 (2012).